Instability of electroconvection in viscoelastic fluids induced by strong unipolar injection between two coaxial cylinders

Zi-Yao Zhang,[1,2,*] Tian-Fu Li,[3,*] Zheng-Gang Su,[1,2] Jian Wu,[1,2] and Hong-Liang Yi[1,2,†]

[1]*School of Energy Science and Engineering, Harbin Institute of Technology, Harbin 150001, People's Republic of China*

[2]*Key Laboratory of Aerospace Thermophysics, Ministry of Industry and Information Technology, Harbin 150001, People's Republic of China*

[3]*Ji Hua Laboratory, Foshan 510006, Guangdong, People's Republic of China*

(Received 29 November 2021; accepted 11 April 2022; published 20 May 2022)

In this paper, a detailed two-dimensional numerical study on the nonlinear behaviors of electrohydrodynamic flows of Oldroyd-B viscoelastic dielectric liquid between two coaxial cylinders is conducted. The liquid is subjected to strong unipolar injection from inner annulus. The entire set of coupled equations, including the Navier-Stokes equations, simplified Maxwell's equations, and constitutive equations, is solved by the finite-volume method. Detailed analyses of elastic effects on the flows are presented with corresponding explanation. A bifurcation mode, namely supercritical bifurcation, has been found comparing to the subcritical bifurcation of Newtonian fluids. The linear stability criteria and nonlinear ones corresponding to the onset and stop of the flow motion, respectively, are presented under different elastic conditions. Comparing to Newtonian fluids, the linear stability criteria do not change at low Weissenberg number and decline when Weissenberg number is more than 1, and the nonlinear criteria are larger than that of Newtonian fluids. In addition, viscoelastic fluids show more dynamic behaviors. For example, two charge-void regions rotate in the domain because of azimuthal stress. Due to the first principal normal stress, two parts of charge-void regions first rotate to each other and then are pushed apart. These behaviors are explained in detail and are closely related to the elastic effects.

DOI: 10.1103/PhysRevFluids.7.053701

I. INTRODUCTION

Electrohydrodynamics (EHD) [1,2] is a multidisciplinary phenomenon dealing with interactions of electric field and hydrodynamics. The investigation of EHD in a dielectric liquid subjected to unipolar injection of ions is one of classic problems in EHD, which is called electroconvection mainly driven by Coulomb force and is a general phenomenon in such mediums same as Rayleigh-Bénard convection in nonisothermal fluid [3], has received extensive attention in the past few decades [4]. When the metallic electrodes are immersed in low-conductivity dielectric liquid, the free charges are injected into the liquid at the interface between the liquid and the electrodes, due to the difference in electric potential, which results in the motion of fluid [5–7]. EHD happens widely in nature, and because of its easy controlling and fast response features, it plays a vital role in many industrial domains, for example, EHD pumps [8], electrostatic precipitators [9], and EHD plumes for heat-transfer enhancement [10]. Additionally, due to the strong coupling between the hydrodynamic and electrical effects in liquids, it is usually extremely difficult to determinate

*These authors contributed equally to this work.
†yihongliang@hit.edu.cn

the electric field and charge-density distribution, because the charges which drift under the electric potential difference are transported by the fluid as well. In addition, there are abundant phenomena in EHD, such as instability, fluid motion transition [11], and bifurcations [12].

Researchers used different kinds of methods to study EHD phenomena, like experiments [13] and theoretical analysis [14], making people understand EHD better. Besides, another method, namely direct numerical simulation (DNS) of EHD, can be used to provide richer information about the whole physical fields. However, DNS on EHD has two main difficulties. The first difficulty is the robust coupling among charges, electric field, and flow field. The second is the strong convection-dominated characteristic of the charge transport equation [12]. The strong numerical diffusion invalidates the method based on the finite difference presented by Castellanos and Atten [15]. Given this matter, Chicón *et al.* [16] developed the particle-in-cell (PIC) method, and then Vázquez *et al.* [17] put the forward flux-corrected transport (FCT) scheme comparing the PIC method with integral form of the charge-density transport equation. After that, many other methods were developed, such as the finite elements combined with the particle-in-cell method,, the finite elements and the flux-corrected transport (FE-FCT) method, the discontinuous Galerkin finite-element method [18,19], the total variation diminishing (TVD) scheme based on the finite-volume method [5,20], and the lattice Boltzmann method [21,22]. These studies make it possible to carry out reliable and accurate DNS on EHD, which has greatly promoted the development of EHD.

Plenty of numerical studies on electroconvection in different geometric configurations have been carried out in recent decades, i.e., parallel plates [23,24], concentric annuli [25,26], and spheres symmetrically placed electrodes [27]. There are two main features of EHD problems in these symmetric models [7]:(1) a potentially unstable hydrostatic state implying a linear instability bifurcation, and (2) the subcritical bifurcation nature. Atten and Moreau [28] firstly predicted the onset of the flow motion in the parallel plates using the linear stability analysis approach. It appears that when the voltage difference between two electrodes is beyond a critical value, the fluid begins to move, and they found that this critical value is related to the injection strength and irrelevant to the dimensionless mobility parameter. Later, the experiment proved this prediction conducted by Lacroix and Atten [29]. And then, Atten and Lacroix [30] investigated the subcritical bifurcation phenomenon in planar configuration under injection condition. In addition, there is another associated phenomenon, the nonlinear stability criterion, which means the stop of the flow motion again when the voltage drops to a critical value. This phenomenon is caused by two transport mechanism of charges, i.e., drifted by the electric field and convection by the velocity of the field of fluid, which also leads to the void regions of charges [31]. Then, the investigation in the experiment conducted by Atten and Lacroix [13] verified the nonlinear phenomenon.

In recent years, there were large quantities of studies on EHD in annulus model given the two features of the annulus EHD problems. One is that there is no lateral-wall effect which may affect the rationality of the results, and the other is the wider application of this configuration in real life. Atten and Elouadie [32] investigated eletroconvection in a dielectric liquid under strong unipolar injection condition comparing with the main results in a planar layer of liquid and found that in wire-cylinder geometry there is a quadratic law $I \propto V^2$ for high applied voltages; however, for moderate applied voltage, the current varies according to a power law $I \propto V^{\alpha}$. Fernandes *et al.* [33,34] firstly studied the various complex flows from the stable hydrostatic state to electroconvective state and finally to chaotic state, finding that with the increasing electric Rayleigh number T (which represents the voltage difference) the number of charged plumes and vortex pairs augments. What is more, they found that the onset of electroconvection starts earlier for inner injection than outer injection; however, the transition to chaotic is later. Thereafter they conducted a study on concentric circular cylinders subjected to unipolar charge injection using the normal-mode instability analysis. Hassen *et al.* [35] had a parametric study on electroconvection between coaxial cylinders considering various parameters including the radius ratio, injection strength, and electric Rayleigh number. The onset criterion of electroconvection was obtained by Wu *et al.* [7] using linear stability analysis and direct numerical simulation, and these two results showed an excellent agreement. They mainly focused on the influence of injection strength on the flow patterns. A detailed investigation into

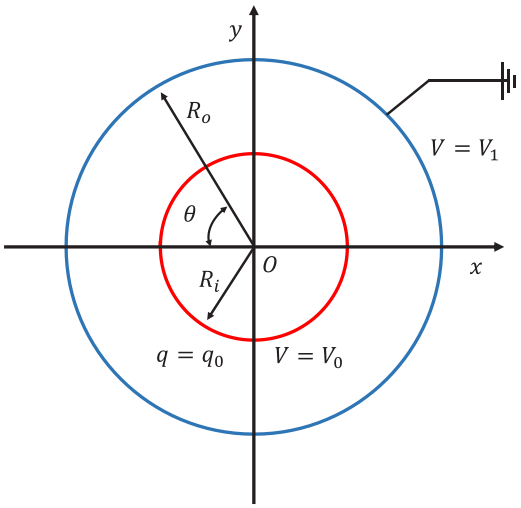

FIG. 1. Sketch of the physical domain and boundary conditions.

subcritical bifurcation and hysteresis loop phenomenon was launched in the finite-amplitude regime between two coaxial cylinders using the finite-volume method and they found that the different complex flow patterns transition is due to the competition of different modes through a simple model analysis. Recently, Huang *et al.* [36,37] investigated the path from the weak steady convective state to chaos in the annuli electroconvective system considering the influence of different radius ratio, the eccentricity, and different mobility parameter.

The fluid types have a great influence on the flow pattern and bifurcation. Viscoelastic fluids as typical non-Newtonians fluids show many unique new phenomena comparing with Newtonian fluid, such as turbulent drag reduction effect [38], and rod climbing phenomenon [39,40], induced by the first principal normal stress difference. There are also many important applications with EHD effects, such as electrospinning [41] which uses electric fields to accelerate and stretch a charged polymer jet. In addition, crude oil could be separated by electric fields from pure water. However, scarce studies of EHD flow subjected to unipolar injection focus on viscoelastic fluids, which largely limits the scope of problem. As more abundant flow patterns exist in viscoelastic fluids, recently, Su [6] *et al.* researched the instability behaviors of viscoelastic fluids subjected to unipolar injection, finding that supercritical bifurcation exits in free-boundary cavity which has no counterpart in Newtonian fluids. Afterwards, Su [42] conducted further research on the effect of nonlinearity of elasticity, finding that there are more abundant transition sequences than those of Newtonian fluids. Li [43] *et al.* had a study on electro-osmotic flow with polymer additives in an electrolyte liquid, which indicates an earlier transition from steady to unsteady convection due to elasticity. Moreover, recently Chen [44] conducted a research of EHD conduction pumping of a viscoelastic fluid, finding that elastic instability is more likely to occur in an Ohmic regime.

Due to two benefits of annulus discussed above, and owing to the rich rheological properties of viscoelastic fluids, it would be natural to expand the electroconvection of Newtonian fluids to viscoelastic fluids in annuli. In this paper, we mainly focus on investigating the effect of elasticity on bifurcation behaviors and its influence on the flow. In addition, there is rare stability analysis work about linear and nonlinear stability criteria of viscoelastic fluids under effect of electric field. Thus, the following linear and nonlinear criteria gotten from numerical results in this paper could serve as the reference of stability analysis. The remainder of this paper is organized as follows. In Sec. II the physical problem, governing equations, boundary conditions, initial conditions, and numerical methods are stated. Section III gives the results of model verification using lid-driven flow

and hydrostatic solution of electroconvection. Then, results and discussions are presented. Finally, a conclusion is drawn in Sec. IV.

II. PROBLEM FORMULATION

A. Physical problem and governing equations

The system under consideration is a layer of dielectric liquid bounded between two concentric infinite cylinders of radius R_o and R_i, respectively (as shown in Fig. 1). We focus on the viscoelastic fluids with constant physical properties such as density ρ_0, dynamic viscosity η, permittivity ε, and ion mobility K, which are assumed to be incompressible and perfectly insulating. The autonomously and homogeneously unipolar inner injection is considered, which means that the charge density injected from the emitter electrode is neither influenced by the electric field nor by the liquid motion and always equals to q_0. The inner emitter electrode is held at V_0 while the outer collector electrode is held at V_1, and this electrical potential difference $\Delta V = V_0 - V_1$ will induce a radial electric field $\vec{E}$ and charge injection into the bulk. And, here is the set of governing equations [5–7]:

$$\nabla \cdot \overrightarrow{U} = 0, \tag{1}$$

$$\rho_0 \left(\frac{\partial \overrightarrow{U}}{\partial t} + (\overrightarrow{U} \cdot \nabla) \overrightarrow{U} \right) = -\nabla p + \nabla \cdot \tau + \overrightarrow{f_e}, \tag{2}$$

$$\frac{\partial q}{\partial t} + \nabla \cdot \overrightarrow{j} = 0, \tag{3}$$

$$\overrightarrow{E} = -\nabla V, \tag{4}$$

$$\Delta V = -\frac{q}{\varepsilon}. \tag{5}$$

Here, $\overrightarrow{U} \equiv [u,\ v]$ is the fluid velocity, $\vec{E} \equiv [E_x,\ E_y]$ is the electric field vector, q is the charge density, τ is the total extra stress tensor, $\overrightarrow{f_e}$ is the density of the electric force, and $\vec{j}$ is the electrical current density. It is assumed that this quasielectrostatical fluid is nonconducting medium, and also the diffusive processes of free charges could be neglected compared with the migration and convection processes. It is worth noting that α is the nondimensional charge-diffusion number and is typically in the range of 10^{-4} to 10^{-3} [45]. With this assumption the charge density could be denoted as [46]

$$\overrightarrow{j} = q\overrightarrow{U} + qK\overrightarrow{E}. \tag{6}$$

Additionally, the electric force could be expressed as [5]

$$\overrightarrow{f_e} = q\overrightarrow{E} - \frac{E^2}{2}\nabla\varepsilon + \nabla\left[\frac{E^2}{2}\rho\frac{\partial\varepsilon}{\partial\rho}\right]. \tag{7}$$

Since the viscous dissipation and Joule heating are very small [46], we can consider the fluids as being isothermal and homogeneous, so the dielectric force, namely the second term including in the electric force vanishes, and we can include the third term, namely the electrostriction force, in the pressure gradient term to simplify the momentum equation [5]. Because the fluid is viscoelastic, the total extra stress tensor τ can be denoted as the sum of a polymer stress τ_p with a solvent stress τ_s. In this paper, the rheology of the polymer is approximated by the Oldroyd-B constitutive model in order to exclude the influences of other factors such as shear thinning [6]. Thus, the solvent stress could be written as $\tau_s = \eta_s[\nabla\vec{U} + (\nabla\overrightarrow{U})^{\mathrm{T}}]$ and the polymer stress $\tau_p = \eta_p(C-I)/\lambda$. Here, η_s and η_p refer to the solvent dynamic viscosity and polymeric dynamic viscosity, respectively, λ denotes the relaxation time of the polymers, and $\boldsymbol{C}$ is the conformation tensor, which has the

same dimensionless form. In addition, the dynamic viscosity of the fluid could be expressed as $\eta = \eta_s + \eta_p$, and the conformation tensor transport equation is

$$\frac{\partial \boldsymbol{C}}{\partial t} + \overrightarrow{U} \cdot \nabla \boldsymbol{C} = \boldsymbol{C} \cdot \nabla \overrightarrow{U} + \boldsymbol{C} \cdot \nabla \overrightarrow{U}^{\mathbf{T}} - \frac{1}{\lambda}[\boldsymbol{C} - \mathrm{I}]. \tag{8}$$

It is particularly convenient to work with nondimensional equations for describing the problem universally. Here, we introduce the interelectrode spacing $L = (R_o - R_i)$ for length normalization, ΔV for electrical potential, ionic velocity scale $K\Delta V/L$ for velocity, q_0 for charge density, $\rho K^2 \Delta V^2/L^2$ for pressure, $L^2/K\Delta V$ for time, and $\Delta V/L$ for electrical field, and the conformation tensor is a nondimensional physical variable, which leads to the following sets of nondimensional equations (for clarity, the superscript asterisk for nondimensional variables is omitted):

Continuity equation:

$$\nabla \cdot \overrightarrow{U} = 0. \tag{9}$$

Momentum conservation equation:

$$\frac{\partial \overrightarrow{U}}{\partial t} + (\overrightarrow{U} \cdot \nabla)\overrightarrow{U} = -\nabla p + \frac{\beta}{T/M^2}\Delta \overrightarrow{U} + \frac{1-\beta}{Wi \cdot T/M^2}\nabla \cdot \boldsymbol{C} + CM^2 q \overrightarrow{E}. \tag{10}$$

Poisson equation:

$$\Delta V = -Cq. \tag{11}$$

Electric potential equation:

$$\overrightarrow{E} = -\nabla V \tag{12}$$

Charge transport equation:

$$\frac{\partial q}{\partial t} + \nabla \cdot (q(\overrightarrow{U} + \overrightarrow{E})) = 0. \tag{13}$$

Conformation transport equation:

$$\frac{\partial \boldsymbol{C}}{\partial t} + \overrightarrow{U} \cdot \nabla \boldsymbol{C} = \boldsymbol{C} \cdot \nabla \overrightarrow{U} + \boldsymbol{C} \cdot \nabla \overrightarrow{U}^{\mathbf{T}} - \frac{1}{Wi}[\boldsymbol{C} - \mathrm{I}]. \tag{14}$$

From the above set of equations, there are several dimensionless numbers relevant to this problem:

$$T = \frac{\varepsilon(V_0 - V_1)}{\eta K}, C = \frac{q_0 L^2}{\varepsilon(V_0 - V_1)}, M = \frac{1}{K}\left(\frac{\varepsilon}{\rho}\right)^{1/2}, Wi = \frac{\lambda U_0}{L}, \beta = \frac{\eta_s}{\eta_s + \eta_p}, \tag{15}$$

where the electric Rayleigh number T represents the ratio of Coulomb and viscous forces, which denotes the intensity of the dominated driving force; C is the dimensionless measure of the injection level representing the charge injection intensity. According to the definition in Ref. [47], the injection level could be divided into three regimes from weak level to strong: weak ($C < 0.2$), medium ($0.2 < C < 5$), and strong ($C > 5$). M is defined as the ratio between the so-called hydrodynamic mobility and the true mobility, and it totally depends on the nature of the fluid and the ion; Wi is Weissenberg number representing the ratio of relaxation time of the viscoelastic fluids to the characteristic time of the flow; and β denotes the ratio of the solvent viscosity to the total viscosity. In addition, we define the radius ratio $\Gamma = R_i/R_o$ to describe this concentric annulus problem.

B. Boundary and initial conditions

The nondimensional computational domain is bounded within the annulus $0 \leqslant \theta \leqslant 2\pi$ and $R_i \leqslant r \leqslant R_o$. For both inner and outer electrodes, no-slip boundary conditions are applied. On

TABLE I. A_e and B_e coefficients of the hydrostatic solution. The bold values are to highlight the case under consideration in this paper, $\eta = 0.5$.

η	0.1	0.2	0.3	0.4	**0.5**	0.6	0.7	0.8	0.9
A_e	1.009	1.099	1.193	1.302	**1.439**	1.622	1.886	2.325	3.309
B_e	−0.0022	−0.050	−0.169	−0.427	**−0.979**	−2.224	−5.409	−15.946	−80.890

the inner emitter electrode, $V = V_0 = 1$ and $q = q_0 = 1$ are set; on the outer collecting cylinder, V and the normal gradient for q are set as zero. In addition, the conformation tensor components on the boundary are obtained by linear extrapolation.

Since the whole set of equations is time dependent, initial conditions should be given. Generally, we could start from the fluid with all variables being zero, the hydrostatic state or the steady state gotten from previous simulations. The hydrostatic solution corresponds to the analytical solution in the case where the fluid velocity is taken as zero, and it could be expressed as [46]

$$q_s(r) = A_e[\delta(r^2 + B_e)]^{-(1/2)}, \tag{16}$$

where $\delta = +1$ and -1 for the inner and outer injections, respectively. A_e and B_e depend on the radius ratio Γ, injection level C, and the injection direction. In this paper we just consider inner injection, and Table I lists the values of A_e and B_e when $C = 10$.

C. Numerical methods

It is worth noting that the hyperbolic nature of charge density and conformation tensor transport equations make the problem more nonlinear, resulting in more difficulties in numerical simulation. In this paper, the whole set of coupled partial differential equations [Eqs. (9)–(14)] is solved using the finite-volume method in the open-source OPENFOAM® toolbox [48,49]. The whole domain is discretized with uniform constructed grids consisting of nonorthogonal quadrilaterals. In the discretization scheme, the second-order central difference scheme is used to discretized the diffusion terms, and the second-order semi-implicit scheme is used to discretize the variables related with the time. Additionally, the semi-implicit method for pressure-linked equations-consistent algorithm [50] is adopted for the decoupling of velocity and pressure. Due to the hyperbolic nature of charge density and conformation tensor transport equations, we pay special attention to the convective term in both equations.

Because the diffusion term in the charge transport equation could be ignored, it becomes the typical hyperbolic equation which is strong convection prevailed. To avoid the large numerical diffusion from the low-order formats or nonphysical oscillations induced by higher-order formats, we use the total variation diminishing scheme (TVD) [5] to deal with the convective term of the charge transport equation. And, TVD was proved to be efficient in simulation of the charge transport by Traoré and Pérez [5], which could capture the steep gradient of charge density and avoid unphysical oscillations.

Considering the constitutional governing equation of conformation tensor, some numerical methods proposed by Pimenta and Alves [49] have been used to treat it because of its hyperbolic nature. Firstly, given the coupling between the extra stress and velocity, a stress-velocity coupling method (see Ref. [49] for details) is introduced to solve the problem which is the similar to pressure-velocity problem. Secondly, in order to solve the high Weissenberg numbers (Wi) problem resulting from the exponential growth of stresses with the increasing of Wi, we use the log-conformation representation to transform the conformation tensor transport equation. By using the method, the symmetry and positive definiteness of conformation tensor could be maintained, and it can also capture higher stress gradients at a high Wi value by linearizing the exponential growth; for a detailed introduction of log-conformation representation please refer to Refs. [51,52]. In addition, the convergent and universally bounded interpolation scheme for the treatment of advection (CUBISTA) [53] is widely

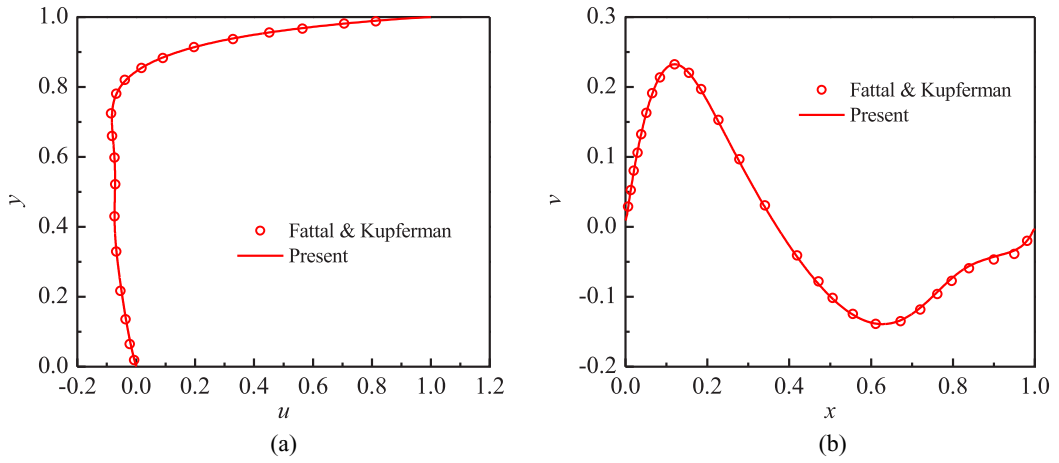

FIG. 2. Comparison of velocity profiles in lid-driven cavity along the lines $x = 0.5$ and $y = 0.75$ at time $t = 8$ for $Wi = 2.0$ and $\beta = 0.5$.

used in non-Newtonian problems for the conformation transport equation, so it is used to discretize the convective term in conformation tensor transport equation.

III. RESULTS AND DISCUSSION

In this paper, we mainly focus on the strong injection case with $C = 10$ and $M = 10$, which is always taken into consideration with parallel plates, concentric annuli, and spheres symmetrically placed electrodes configuration. It could be approximately compared to space-charge limited regime, which is defined as $C \gg 1$ [13] and usually adopted in experiments. We fix the radius ratio Γ to 0.5 (namely, $R_o = 2$ and $R_i = 1$), and only consider the case that the injection is induced from the inner electrodes. Viscoelastic fluids are considered and the value of β is fixed at 0.8. A detailed examination of bifurcation processes, charge distributions, as well as flow patterns under different elastic effects has been carried out. Notably, the results of Newtonian fluids under similar geometric configuration were well presented in Ref. [7], which could serve as a reference for comparison.

A. Code and model verification

The correctness and precision of the solver adopted in this work are validated by separately verifying the viscoelastic and electrical parts. First, consider a benchmark test of viscoelastic fluids simulation, namely, the extensively studied problem about lid-driven cavity flow. The fluid in the cavity is driven by the moving of upper lid, and we compare our results with those in Ref. [51]. The case when $Wi\ (\equiv \lambda U/H) = 2$, $\beta = 0.5$, and $Re\ (\equiv \rho UH/\eta) \to 0$, is computed. Figure 2 shows the velocity profiles along the lines $x = 0.5$ and $y = 0.75$ (dimensionless length) at time $t = 8$. It appears that our results are in good agreement with those in Ref. [51].

Secondly, in the validation of the electrical part, the strong injection of $C = 10$ and $M = 10$ in the annulus model is studied. The according analytical solution of charge distribution in the hydrostatic regime has been given in Eq. (16) and relevant parameters are presented in Table I. We consider the concentric annulus when $\Gamma = 0.5$. The charge-density profiles are shown in Fig. 3 obtained from different grid sizes of 300×120, 400×150, and 400×200. It is worth noting that the numerical results computing from our codes are in great accordance with the analytical solutions even for the coarsest grid of 300×120. In the remainder of the paper, fluid motion starts from the hydrostatic state unless otherwise stated. In addition, in order to confirm the validity of the code of the electrical part, the maximum velocities and the electrical Nusselt number (Ne is defined as the ratio of the

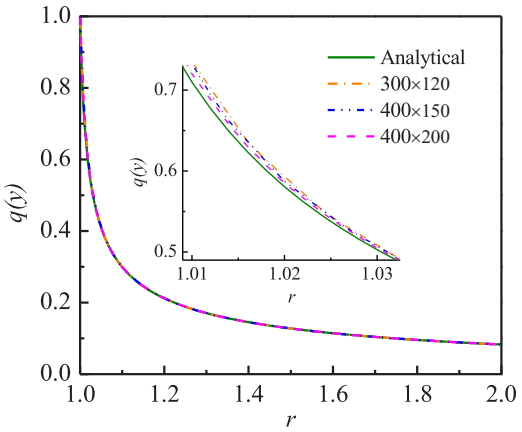

FIG. 3. Charge-density profile obtained in the hydrostatic regime under different grid sizes, computed numerically and compared to the analytical solution.

total current I_e to the conductive current I_0) have been given in Table II compared with the results of Wu and Traoré [54] (the results given in Table 2 of their paper). It could be found that our results show a great agreement with the results in their paper considering the currents. So, the electrical module has been sufficiently proved.

B. Weakly elastic fluids

The weakly elastic effect with $Wi = 0.1$ is first selected to make a preliminary comparison with the Newtonian fluids. According to the instability phenomenon under the condition with Newtonian fluids, when the driving parameter is near the linear bifurcation criterion, the perturbations of relevant physical quantity f follow the exponential law $f = f_0 e^{\sigma t}$ [5]. The growth rate σ is positive above the instability threshold and negative below it, so we can get the linear criterion by examining the growth rate. Moreover, it has been reported that the perturbations of electroconvection in viscoelastic fluids still follow this exponential growth law [6]. In this paper, the maximum value of the velocity $v_{\max} = \overrightarrow{U}_{\max} \cdot \overrightarrow{e}_y$ is taken as the representative physical quantity. Figure 4 shows the velocity profiles: $\log(v_{\max})$ versus t evolution processes with $Wi = 0.1$. It could be found that near the critical value of T, the growth rate σ is a linear function of T. Thus, a linear fitting of the curve $\sigma(T)$ is used to obtain the linear criterion, and $T_c = 123.6$ could be found when $\sigma = 0$. This is in good accordance with the critical value of Newtonian fluids, which is 122.84 [7] theoretically and 123.06 obtained by numerical study of Wu [7]. From the velocity profiles, it could be discovered that the growth curves of velocity eventually tend to the same growth stage with the increasing of T, because when T increases, the motion of fluid will be reinforced, and the nonlinear effect from elasticity and fluid dynamics would have an influence on the first linear growth stage and result it into one. Therefore, it is worth noting that under this parameter region the linear criterion of the

TABLE II. The maximum vertical velocity and the electric Nusselt number for various M for $T = 190$.

M	3	5	10	20	50
$v_{\max}$ (Present)	3.143	3.515	3.751	3.803	3.818
$v_{\max}$ (Wu *et al.*)	3.146	3.520	3.755	3.807	3.822
Ne (Present)	1.486	1.493	1.530	1.543	1.548
Ne (Wu *et al.*)	1.492	1.497	1.535	1.548	1.552

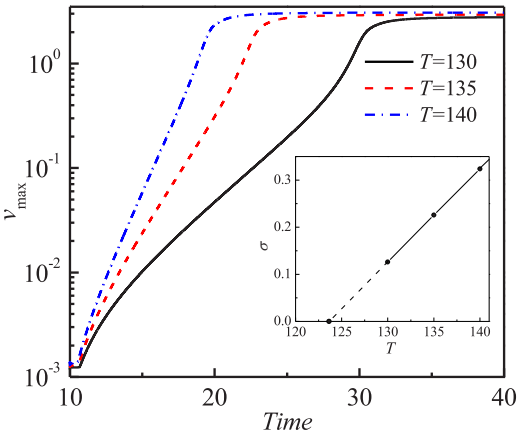

FIG. 4. Temporal evolutions of the maximum velocity in the logarithmic coordinate, $Wi = 0.1$.

viscoelastic fluid is identical to that of Newtonian fluids, and it is the same as what Su [6] obtained in the parallel plate model. It was pointed out by Larson [55] that a simple type of viscoelastic fluids becomes Newtonian when the motion of fluid is weak and stable, which is in agreement with our result.

Next, the bifurcation process under weakly elastic effect with $Wi = 0.1$ is examined. As shown in Fig. 5, by increasing T, when T is below the linear criterion, the small perturbations of velocity will be dissipated by the viscous effect and elastic effect which could be neglected under this weak motion comparing with viscous torque, so the fluid remains static. When T increases to the critical value, the Coulomb force acts like a torque to speed up the flow. To briefly introduce this process, we assume a small perturbation of velocity in the computation domain. Considering a vortex in the system, on the one side, the Coulomb force overcomes the effect of viscosity at these domains where the flow direction is identical to the drift direction of free charges, and then the charge density near this region increases inducing larger Coulomb force, while on the other side, the flow direction is reversed, and the region void of charge will exist when the flow velocity is larger than the ion drift velocity, which is a very important feature of electroconvection problems. In addition, the ion drift exists all the time, so the flow velocity will be stable at a finite velocity value, which is another characteristic feature of EHD, namely, subcritical bifurcation.

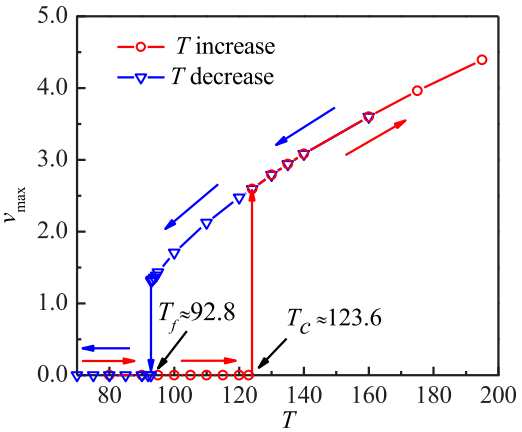

FIG. 5. Hysteresis loop represented by the maximum velocity v_{max}, $Wi = 0.1$.

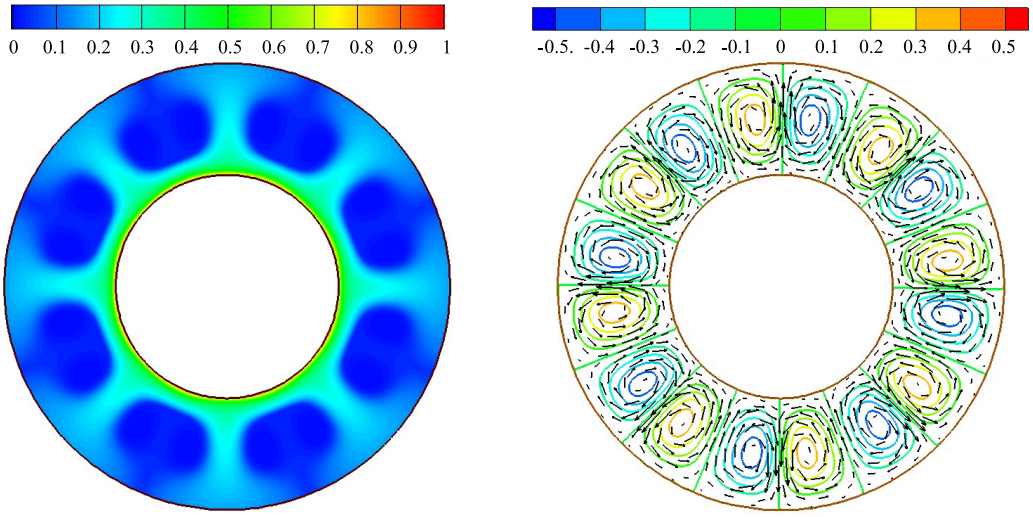

FIG. 6. Distributions of (a) charge density and (b) stream function and velocity field with $T = 130$, $Wi = 0.1$.

As an example, the charge density and streamline distributions for $T = 130$ are presented in Fig. 6. Differ from what Wu reported in Ref. [7], where the steady state could be of seven or eight pairs of vortices through different development paths for Newtonian fluids. For viscoelastic fluids, it is always of the eight-pairs steady flow pattern through the paths under the same parameters. Then in Fig. 5, we gradually increase T, and it could be obviously found that with the increment of T, the maximum velocity grows. As we reduce T from the result of $T = 185$, the fluid does not get to rest when T is slightly below T_c. This is because the maximum convective velocity is still larger than ion drift velocity, and a hysteresis loop is traced. The same phenomenon that the charge-void regions shrink when we incessantly decrease T compared with Newtonian fluids happens considering viscoelastic fluids. However, when T is close to 92.8, the fluid motion stops suddenly, which corresponds to the nonlinear criterion. The nonlinear criterion value is slightly higher than that of Newtonian fluids [7], and this is identical to the trend gotten by Su [6] which is also slightly higher in parallel plates model. With the decreasing of T, the flow velocity goes down, and then the flow returns to rest and remains stable at hydrostatic state. Due to the effect of elastic stress, the flow velocity gets slower than that of Newtonian fluids under the same situation, as shown in Fig. 7. It can be seen that in the middle of the charge-void regions, the first principal normal stress is positive, which means the elastic stress in the radial direction is dominant, and it suppresses the motion of the fluid in the radial direction. Thus, when $T = 92.8$, the flow returns to rest, while under the parameters the elastic effect is weak, resulting in a slightly larger nonlinear criterion.

C. Moderately elastic fluids

When the elastic effect is weak, the corresponding bifurcation process is similar to that of Newtonian fluids. However, when the elastic effect becomes stronger, the bifurcation process is quite different. In this subsection, we have a detailed examination of flow bifurcation of moderate elastic effect. In these moderate elastic fluids, the exponential growth region has been submerged by oscillation. Therefore, dichotomy is used to confirm the linear stability criteria. When the value of Wi increases to 0.4, it could be observed in Fig. 8 that the maximum vertical velocity increases

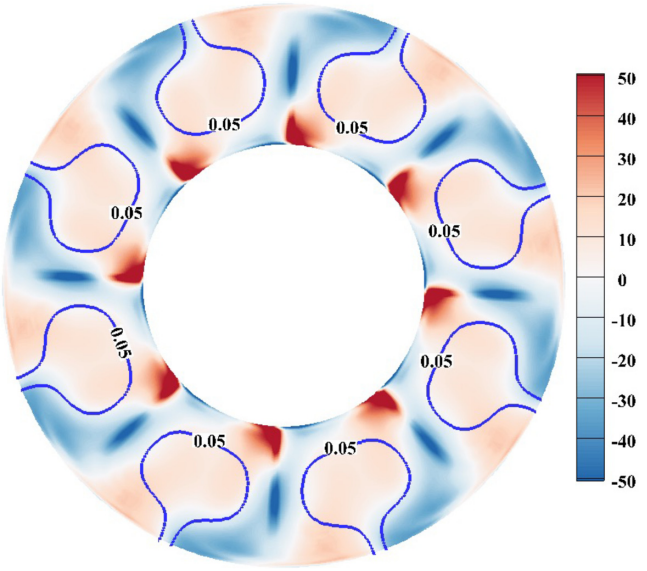

FIG. 7. Distributions of first principal normal stress with $T = 130$, $Wi = 0.1$. Note: we show the contour line of charge density where $q \leqslant 0.05$, which represents the charge-void regions.

continuously with the growth of T at first, which means the supercritical bifurcation happens at first, and the flow stays stable in this small region (from $T = 123.6$ to $T = 125.3$). The typical charge distribution with its stream function in this region is presented in the inset of Fig. 8, where it could be discovered that the charge-void regions are not formed yet, because in the small region the flow is weak, and the convection of charge is weaker than the drift effect. It is mainly because the polymeric stress torque could help the electrical torque compete with viscous torque, which makes these solutions (namely $0 < \overrightarrow{U} < K\vec{E}$) possible. Moreover, the corresponding eight pairs of vortices could be discovered through the inset.

By further increasing the value of T, the velocity drastically increases and jumps into a larger branch with the flow unstable at $T = 125.3$ as a secondary bifurcation, and each velocity point in Fig. 8 is time-averaged value when T is bigger than 125.3. In order to describe the corresponding

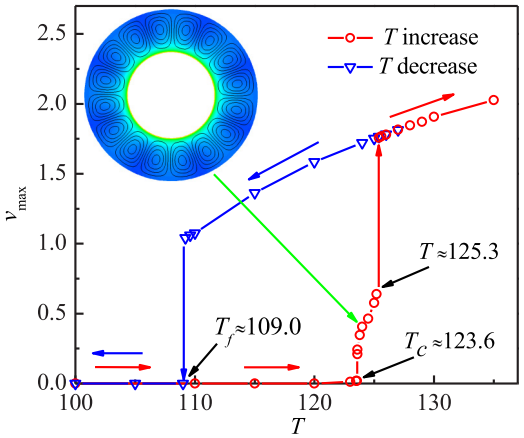

FIG. 8. Bifurcation diagram for $Wi = 0.4$ represented by the maximum velocity $v_{\max}$.

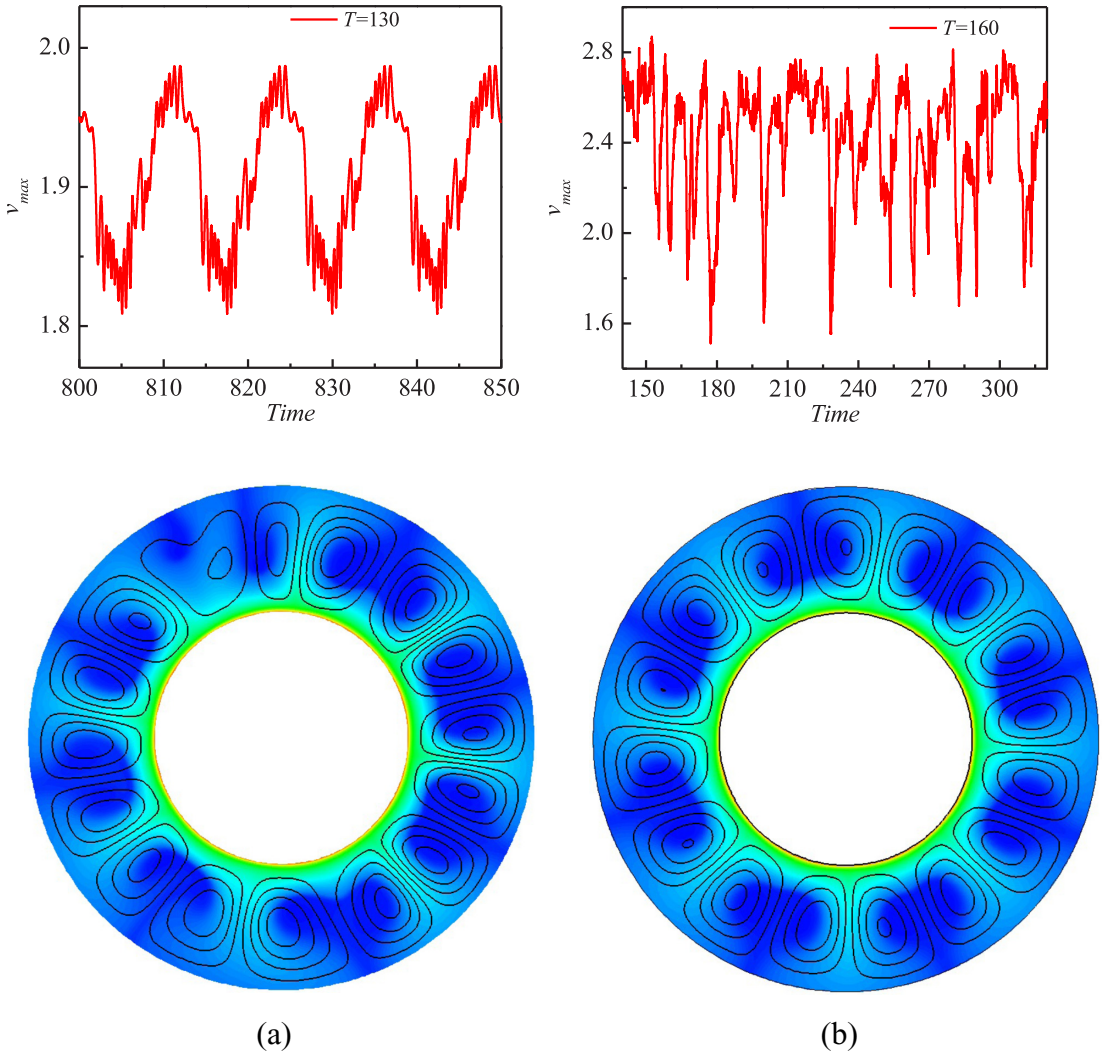

FIG. 9. Distributions of charge density and stream function with temporal evolution of $v_{\max}$ for $Wi = 0.4$ (a) $T = 130$ at $t = 810$ and (b) $T = 160$ at $t = 250$.

flow state more clearly, the time evolutions of $v_{\max}$ as well as charge-density distributions with stream function at different times for typical cases with $T = 130$ and $T = 160$ have been presented in Fig. 9. It could be found from Fig. 9(a) that an oscillatory flow with eight pairs of vortices is at $T = 130$, which corresponds to eight asymmetric charge-void regions swinging within a small domain, and the frequency spectrum analysis (see Fig. 14) of the temporal evolution of its corresponding $v_{\max}$ shows that the flow is periodic. Further increasing the value of T, as shown in Fig. 9(b), we observe that a large charge-void region splits into two little ones when $T = 160$. It is pretty different from Newtonian fluids that are totally stable state under this parameter. In addition, the change of velocity no longer shows the law of periodic oscillation, but tends to chaos. Due to the fact, we think that elasticity has significant influence on the stability of fluids. For larger values of T, the pairs of vortices increase and change within a certain amount, and the flow changes into completely random state, which is beyond the scope of this paper.

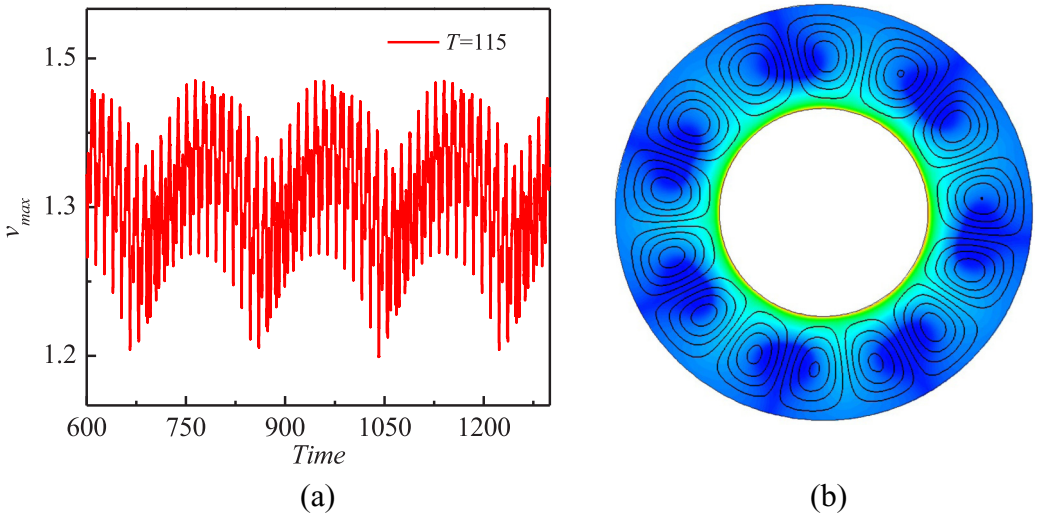

FIG. 10. (a) Temporal evolution of $v_{\max}$ and (b) distributions of charge density with stream function for $T = 115$ when $Wi = 0.4$.

When T decreases, the hysteresis loop still remains, as shown in Fig. 8. It is worth noting that this bifurcation process is similar to what Su [6] reported in cavity with rigid walls cases, and it could be found that the stable-state region is much larger than ours, while this stable region is not permissible for annuli with Newtonian fluids. By further reducing T, comparing with the results in Ref. [6], it shows abundant flow patterns rather than returning to steady state without lateral-wall effect, and the nonlinear criterion is $T_f = 109.0$. Since the flow shows the subcritical bifurcation nature, it is of great significance to investigate the flow behavior under the linear criterion. It should be noted that when we reduce T from 130 to 120, eight pairs of oscillatory vortices with corresponding eight charge-void regions are found, which is similar to the result of $T = 130$, as shown in Fig. 9(a). This means that the hysteresis loop nature does not change yet and the fluid motion does not return to steady state again comparing to the fluid with low Weissenberg number. This behavior maintains until $T = 115$. When T decreases to 115, only seven pairs of oscillatory vortices remain, as shown in Fig. 10 with according temporal evolution of $v_{\max}$. Additionally, the corresponding seven charge-void regions still swing within a small domain. As T is further reduced to $T = 112$, only four charge-void regions remain in the domain, and as the number of charge-void regions decreases, the swinging amplitude is enlarged for each one combining with the development and vanishment of pairs of vortexes, as shown in Fig. 11. Then, continuing to reduce the value of T to 110, the flow field is switched to two charge-void regions rotating in the domain as can be seen in Fig. 12.

Here, we will give the corresponding explanation on above behaviors. When T decreases, the number of charge-void regions decreases, and this is because in this process, the electric effect is weakened, and the elastic effect is suppressed at the same time, resulting in the reduction of convection velocity. This is similar to the convection in parallel plates with large aspect ratios where the electric torque competes with the viscous torque, and due to the decrease of the convection velocity, the charge-void regions decline. Considering the rod-climbing phenomenon [40], the mainstream is azimuthal direction, and it induces the radial stress, namely, the volume force induced by the first principal normal stress. Comparing to the rod-climbing phenomenon, when $T = 112$, the mainstream of this motion is in the radial direction. Thus, when the left two charge-void regions rotate towards the two right ones (a, b towards c, d), due to the high value of the first principal stress between the left and right parts of charge-void regions (in the middle of a, b and c, d), as shown in Fig. 13(a), it induces the azimuthal stress which is perpendicular to the mainstream

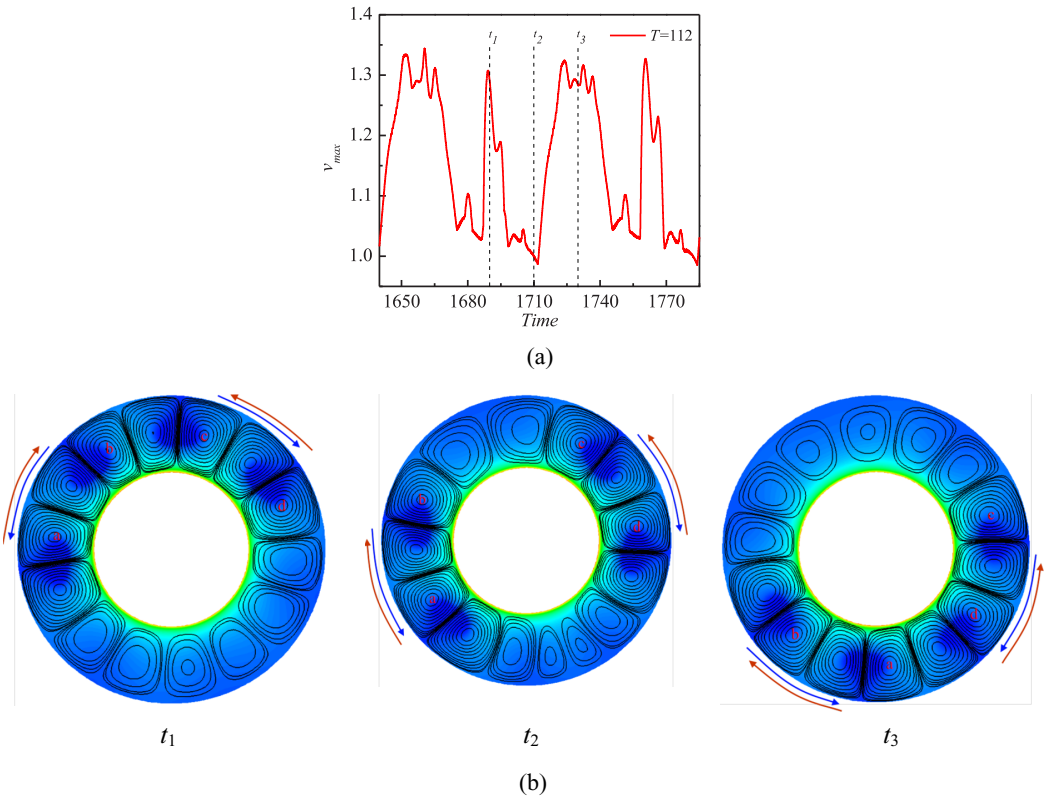

FIG. 11. (a) Temporal evolution of $v_{\max}$ and (b) distributions of charge density with stream function for $T = 112$ when $Wi = 0.4$. Note: The charge-void regions move following the direction of the blue arrow at first and turn back following the red arrow.

direction to push the adjacent charge void regions apart. Similar description has been used to explain pushing heat plumes apart [56]. It is worth noting that this rotating phenomenon when $T = 110$ was found by Huang *et al.* [36] in eccentric annuli. It is explained that the eccentricity leads to the asymmetry of electric field, resulting in a difference of electrical torque that induces the rotating flow. Nevertheless, considering our symmetric model, as shown in Fig. 13(b), the azimuthal stress sets the flow into anticlockwise rotating represented by positive value in the image, and equals to 3.765 in nondimensional value by summing up the elastic torque, which means that it induces the flow rotate anticlockwise.

To further explain the flow behaviors in this system, the trajectory of the velocity at sample point is shown in Fig. 14, and the sample point A is at (1.5, 0). Through Fig. 14(a), a closed loop is displayed, and it could be found that there is one main peak frequency, which shows a characteristic of periodic flow. The fundamental frequency at $T = 130$ is $f = 0.0804$, while when $T = 115$ and 112, it could be discovered through temporal velocity images that they are quasiperiodic flows, and the flow patterns which change from swinging in the little regions to rotating are different from those of $T = 130$. Note that when $T = 110$, the flow transforms to periodic state with fundamental frequency of $f = 0.0053$; this result is not presented here for space limitations. Eventually, the flow returns to rest at $T = 109.0$, which is much higher than the nonlinear criterion for the case of $Wi = 0.1$. Moreover, as the nonlinear criterion increases with Wi while the linear criterion stays the same, it indicates that the nonlinear criterion will coincide with the linear criterion by increasing Wi, which will be presented later when $Wi = 0.7$.

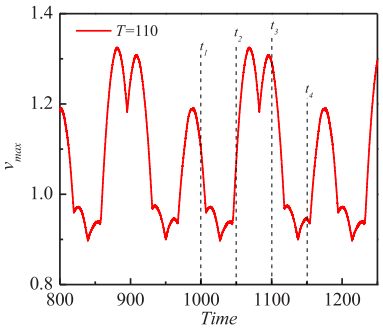

(a)

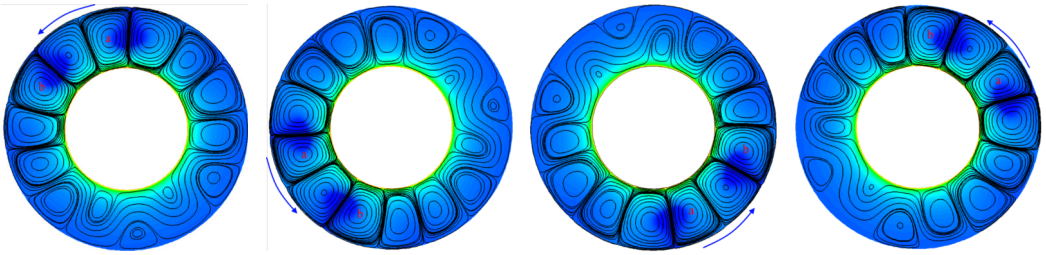

(b)

FIG. 12. (a) Temporal evolution of $v_{\max}$ and (b) distributions of charge density with stream function for $T = 110$ when $Wi = 0.4$. Note: The charge-void regions rotate following the direction of the blue arrow.

Next, we examine the solutions when $Wi = 0.7$, as shown in Fig. 15; the supercritical bifurcation happens with stable state in the low-velocity branch at $T_c = 123.6$ as well. With the increasing of T, the stable state is maintained until $T = 126.3$. Then, the flow becomes unstable at $T = 126.3$. It is intriguing that the hysteresis loop vanishes and the velocity decreases along the same path when T is reduced from the upper branch, which is quite different from rigid-wall cases of Newtonian fluids found by Wu [4] and viscoelastic fluids reported by Su [6]. In the inset of Fig. 15, the typical charge distribution with stream function of stable state in the stable region is given, and eight pairs of vortices indicated by the charge distribution can be observed. Similarly, the charge-void regions are formed on the upper branch. The Fourier frequency spectrum of velocity at sample point A of $T = 135$ is also shown in the inset of Fig. 15. It can be seen from the inset that the flow is very chaotic. In addition, after increasing T to the unstable branch, the charge distributions are similar to the random state at $T = 160$ for $Wi = 0.4$ [see Fig. 9(b)], while this phenomenon does not happen at the same low driving parameter for Newtonian fluids [7]. This elastic instability [57] phenomenon at low Reynolds number happens widely in viscoelastic fluids, and could be applied in enhancement of mass transfer.

D. Strongly elastic fluids

In this subsection, the strongly elastic fluids with $Wi \geqslant 1$ are considered. First, compared with $Wi = 0.4$ and 0.7, when the value of Wi number is increased to 1, the bifurcation process has turned back into subcritical bifurcation again, as shown in Fig. 16(a). It is worth noting that each point in this process is unstable and we get corresponding time-averaged value, which is quite different from the case of Newtonian fluid or fluid with low Wi. It could be found that the maximum velocity of different T values is also much lower than that of Newtonian fluids or lower Weissenberg numbers.

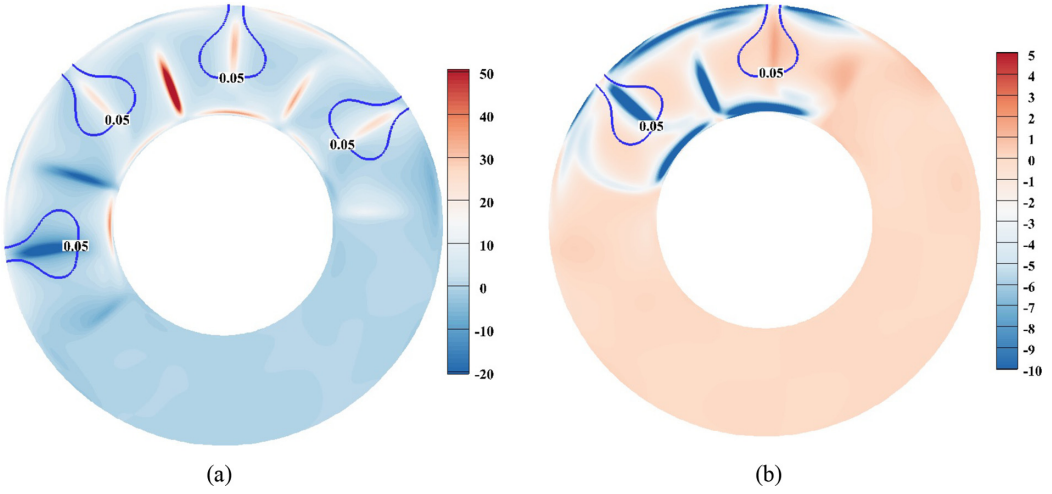

FIG. 13. (a) Distributions of first principal normal stress for $T = 112$ and (b) elastic stress in the azimuthal direction for $T = 110$ when $Wi = 0.4$. Note: we show the contour line of charge density where $q \leqslant 0.05$, which we consider as charge-void regions.

This means that the strong elasticity causes the suppression of flow motion, though the flow is quite unstable. Figure 16(b) shows that the velocity experiences an oscillating growing process at the beginning of its evolution, and finally turns into a totally irregular oscillation.

Once the flow is set into motion above the onset criterion, it is in a quite random state with seven pairs of oscillatory vortices with corresponding seven charge-void regions; thus, we focus on the lower values of T. We reduce the T value from the former state, and find that the flow motions are very similar to each other when T is below T_c. Additionally, we show the result of $T = 115$ in Fig. 17 as an example. It appears that the result is a periodic state observing from the temporal evolution of $v_{\max}$ in Fig. 17(a). As shown in Fig. 17(b), there are still seven charge-void regions. From t_1 to t_4 the charge-void regions rotate anticlockwise. In addition, these charge-void regions vanish from t_1 to t_2, and are formed again from t_2 to t_3. Moreover, from t_3 to t_4 the charge-void regions vanish again.

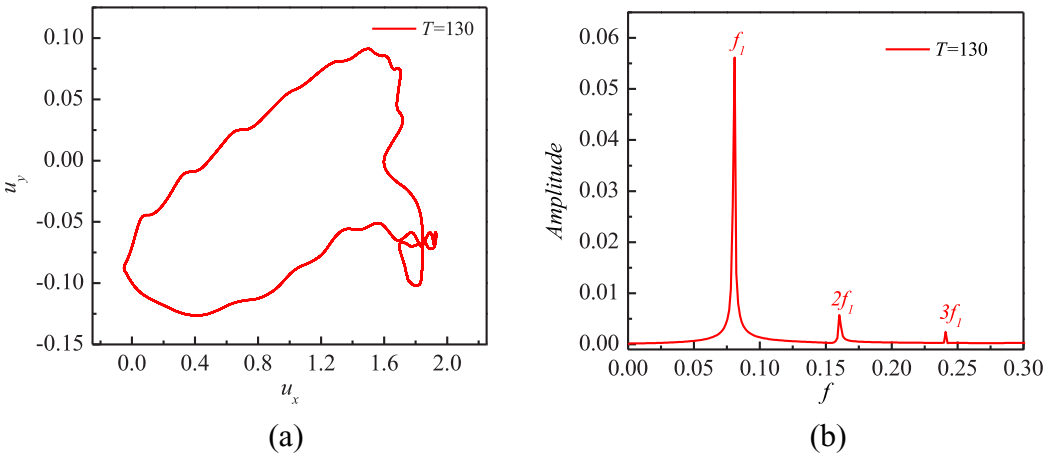

FIG. 14. (a) Phase-space trajectory of the velocity at sample point A and (b) Fourier frequency spectrum of velocity at sample point A for $T = 130$ when $Wi = 0.4$.

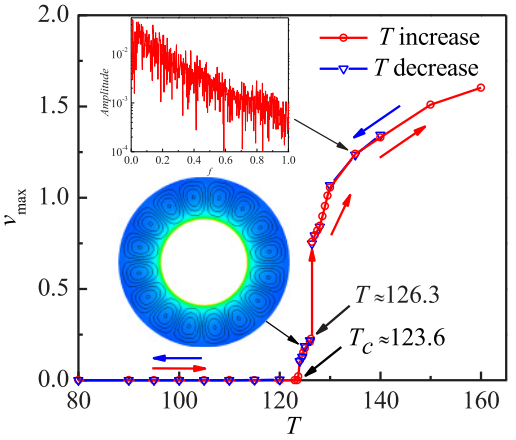

FIG. 15. Bifurcation diagram for $Wi = 0.7$ represented by the maximum velocity $v_{\max}$.

This whole process runs in circle. This rotating phenomenon could be attributed to the azimuthal stress, and the vanishment of charge-void regions is because the convection of charges is weaker than the drift in the according regions.

When the Weissenberg number is larger, ranging from 1 to 5, the system is still of subcritical bifurcation. Due to the fact that the flow patterns vary significantly in these large Wi values, the flow already tends to random state when $Wi = 1$, and considering space limitations we mainly focus on the values of T_c and T_f obtained from our numerical simulations for different values of Wi, which are summarized in Table III. Until today, there is no linear or nonlinear stability analysis about EHD problems of viscoelastic fluids in annuli. We give the corresponding numerical criteria. First, it is shown that when Wi changes from 1 to 2, the two criteria decrease greatly. When $Wi \geqslant 2$, with the increase of Wi the linear and nonlinear criteria decrease slightly. For example, the nonlinear criterion is $T_f = 105.1$ for $Wi = 2$, and $T_f = 103.1$ for $Wi = 5$, showing a difference of 1.9%. This is the maximum difference for T_f that we observed when $Wi \geqslant 2$. The results reveal that the dependence of T_c and T_f on Wi becomes weak with the increase of Wi, and finally they are expected to tend to constants.

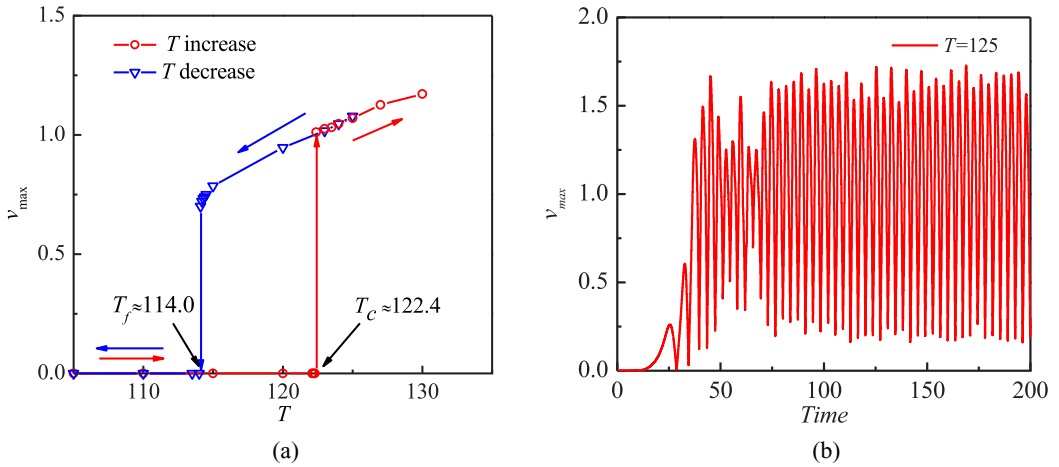

FIG. 16. (a) Bifurcation diagram for $Wi = 1$ and (b) temporal evolution of $v_{\max}$ for $T = 125$.

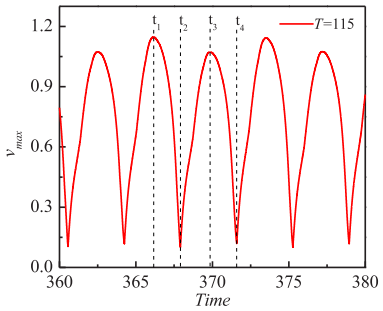

(a)

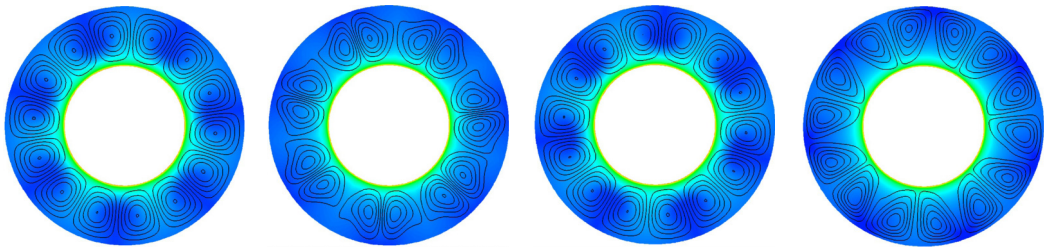

(b)

FIG. 17. (a) Temporal evolution of $v_{\max}$ and (b) distributions of charge density and stream function for $T = 115, Wi = 1$.

E. Variation of onset bifurcation

In order to demonstrate the onset bifurcation more clearly, a flow chart explicitly showing the change of the system due to Wi has been given in Fig. 18. The green spot means the fluid stays in the hydrostatic state under one certain case. The blue triangle means the charge-void regions do not exist but the system already starts to move. The orange rhombus means the charge-void regions exist in the system. Moreover, the symbol line approximately shows the linear criteria and the symbols on the line show the bifurcation types for certain Wi. For example, when $Wi = 0.4$, the bifurcation type changes to supercritical bifurcation. This is because the system could maintain the state without charge-void regions in a range of T after the system starts to move. It is noted that a small range of $T(<125)$ with no charge-void regions is observed but in this range the fluid starts to flow when $Wi = 0.8$ and 0.9, which is the characteristic of supercritical bifurcation. When $Wi \geqslant 1$, the system shows a characteristic of subcritical bifurcation, which means the charge-void regions have been formed after the fluids start to move. What is more, in our work all the changes of system are confirmed by numerical results. Thus, a quantity of computations and analyses should be done for each Wi. Admittedly, a more detailed flow chart could more clearly show the change of the system due to Wi, but it is hard due to the limited computations and analyses.

TABLE III. Dependence of the linear and nonlinear stability criteria on the Weissenberg number Wi.

Weissenberg number, Wi	1	2	3	4	5
Linear (T_c)	122.4	110.2	106.8	104.8	104.0
Nonlinear (T_f)	114.0	105.1	105.2	104.1	103.1

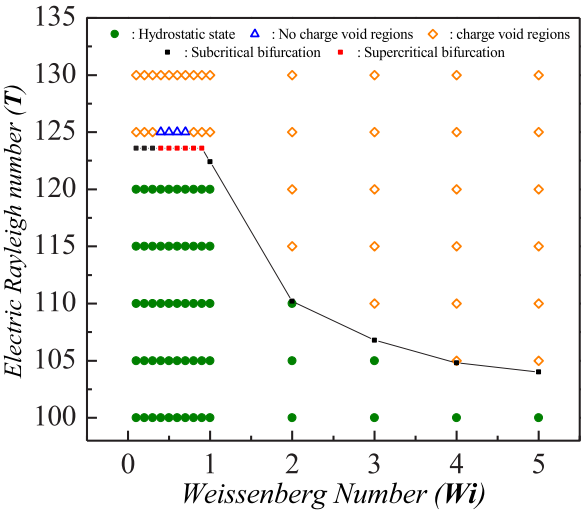

FIG. 18. Flow chart explicitly showing the change of system due to Wi.

IV. CONCLUSIONS

In this paper, the electroconvection in a dielectric viscoelastic liquid between two-dimensional annuli subjected to strong unipolar injection of ions from inner annulus has been investigated in detail. The flow patterns and the bifurcation diagrams have been shown under various Weissenberg numbers.

The results demonstrate that the elastic effect plays an important role in instability modes. It also shows that the bifurcation types of onset and flow patterns will change significantly with the Weissenberg number. When $Wi = 0.1$, the system exhibits subcritical bifurcation, which is the same as the electroconvection of Newtonian fluids, and the linear criterion is the same as well, while the corresponding nonlinear criterion is larger due to the radially dominant first principal normal stress. When $Wi = 0.4$, the supercritical bifurcation happens with a stable state at $T_c = 123.6$, and the subcritical bifurcation continues to happen at $T = 125.3$. When $Wi = 0.7$, the system changes to supercritical bifurcation at the same linear criterion, $T_c = 123.6$. At this time, the hysteresis loop vanishes and the velocity traces back to the former path when T is decreased, which is not observed in classical electroconvection of Newtonian fluids in annuli. When $Wi \geqslant 1$, it has turned back to subcritical bifurcation, and the fluid motion is of unstable state after the flow begins. In addition, with the increase of Wi, the linear stability and nonlinear stability criteria of the system begin to decline. However, the nonlinear stability criteria of viscoelastic liquid in annuli are still larger than that of Newtonian fluids.

On the other hand, the flow patterns are quite different from those of Newtonian fluids. When Wi is below 0.4, it is shown that the flow patterns are very similar to those of Newtonian fluids. Through different development paths, it appears that viscoelastic fluids always show eight charge-void regions in the domain after the onset of flow motion under the cases considered in this paper, which is quite different from Newtonian fluids with seven or eight charge-void regions, while with the increasing of Wi, the flow patterns of charge-void regions change drastically because of the special rheological nature of viscoelastic fluids, and various flow modes caused by azimuthal stress, first principal normal stress, etc. could be found, namely rotation, swinging, splitting, and vanishing. What is more, when Wi is higher, the behaviors of flow motion are the combination of these four fundamental modes. In addition, it appears that the flow will change into unstable state earlier than Newtonian fluids under the same conditions.

In conclusion, the elastic effect leads to instability patterns and richer dynamical behaviors in electroconvection, which does not exist in Newtonian fluids. On the one hand, the bifurcation types are more abundant with different linear and nonlinear criteria. On the other hand, the flows are prone to rotating due to azimuthal stress. Moreover, the elasticity promotes the transition from the steady state to unsteady convection under the considered conditions. Our numerical results may serve as a reference for the upcoming linear stability analysis and weakly nonlinear stability analysis. In the future work, we will investigate the effects of the radius ratio and viscosity ratio on the bifurcation behaviors and flow patterns.

ACKNOWLEDGMENTS

This work is supported by the National Natural Science Foundation of China (Grant No. 52076055), the Fundamental Research Funds for the Central Universities (Grant No. FRFCU5710094020), and Guangdong Basic and Applied Basic Research Foundation (Grant No. 2021A1515110273).

[1] A. Castellanos, *Electrohydrodynamics* (Springer Science & Business Media, Wien, 1998).
[2] A. I. Zhakin, Electrohydrodynamics, Phys. Usp. **55**, 465 (2012).
[3] P. Traoré, A. Pérez, D. Koulova, and H. Romat, Numerical modelling of finite-amplitude electro-thermo-convection in a dielectric liquid layer subjected to both unipolar injection and temperature gradient, J. Fluid Mech. **658**, 279 (2010).
[4] J. Wu, P. Traoré, P. A. Vázquez, and A. T. Pérez, Onset of convection in a finite two-dimensional container due to unipolar injection of ions, Phys. Rev. E **88**, 053018 (2013).
[5] P. Traoré and A. Pérez, Two-dimensional numerical analysis of electroconvection in a dielectric liquid subjected to strong unipolar injection, Phys. Fluids **24**, 037102 (2012).
[6] Z.-G. Su, Y.-M. Zhang, K. Luo, and H.-L. Yi, Instability of electroconvection in viscoelastic fluids subjected to unipolar injection, Phys. Fluids **32**, 104102 (2020).
[7] J. Wu, P. A. Vázquez, P. Traoré, and A. T. Pérez, Finite amplitude electroconvection induced by strong unipolar injection between two coaxial cylinders, Phys. Fluids **26**, 124105 (2014).
[8] Y. Liao, Z. Feng, and X. Zhou, Predicting the pumping effects of electrohydrodynamic (EHD) gas pumps by numerical simulations and quantitative pressure drop vs. flow rate curves, J. Electrost. **96**, 160 (2018).
[9] A. Jaworek, A. Marchewicz, A. Sobczyk, A. Krupa, and T. Czech, Two-stage electrostatic precipitators for the reduction of PM2. 5 particle emission, Prog. Energy Combust. Sci. **67**, 206 (2018).
[10] J. Wu, P. Traoré, C. Louste, L. Dascalescu, F.-B. Tian, and A. T. Pérez, Numerical investigation of electrohydrodynamic plumes for locally enhanced cooling in dielectric liquids, IEEE Trans. Ind. Appl. **51**, 669 (2014).
[11] T.-F. Li, Z.-G. Su, K. Luo, and H.-L. Yi, Transition to chaos in electro-thermo-convection of a dielectric liquid in a square cavity, Phys. Fluids **32**, 013106 (2020).
[12] K. Luo, J. Wu, H.-L. Yi, and H.-P. Tan, Lattice Boltzmann model for Coulomb-driven flows in dielectric liquids, Phys. Rev. E **93**, 023309 (2016).
[13] P. Atten and J. Lacroix, Electrohydrodynamic stability of liquids subjected to unipolar injection: Non linear phenomena, J. Electrost. **5**, 439 (1978).
[14] Z. Feng, M. Zhang, P. A. Vazquez, and C. Shu, Deterministic and stochastic bifurcations in two-dimensional electroconvective flows, J. Fluid Mech. **922**, A20 (2021).
[15] A. Castellanos and P. Atten, Numerical modeling of finite amplitude convection of liquids subjected to unipolar injection, IEEE Trans. Ind. Appl. **IA-23**, 825 (1987).
[16] R. Chicón, A. Castellanos, and E. Martin, Numerical modelling of Coulomb-driven convection in insulating liquids, J. Fluid Mech. **344**, 43 (1997).

[17] P. Vázquez, G. E. Georghiou, and A. Castellanos, Characterization of injection instabilities in electrohydrodynamics by numerical modelling: Comparison of particle in cell and flux corrected transport methods for electroconvection between two plates, J. Phys. D: Appl. Phys. **39**, 2754 (2006).
[18] P. Vázquez, G. E. Georghiou, and A. Castellanos, Numerical analysis of the stability of the electrohydrodynamic (EHD) electroconvection between two plates, J. Phys. D: Appl. Phys. **41**, 175303 (2008).
[19] P. Vázquez and A. Castellanos, Numerical simulation of EHD flows using discontinuous Galerkin finite element methods, Comput. Fluids **84**, 270 (2013).
[20] J. Wu and P. Traoré, A finite-volume method for electro-thermoconvective phenomena in a plane layer of dielectric liquid, Numer. Heat Transfer, Part A **68**, 471 (2015).
[21] K. Luo, H.-L. Yi, H.-P. Tan, and J. Wu, Unified lattice Boltzmann method for electric field–space charge coupled problems in complex geometries and its applications to annular electroconvection, IEEE Trans. Ind. Appl. **53**, 3995 (2017).
[22] K. Luo, J. Wu, H.-L. Yi, L.-H. Liu, and H.-P. Tan, Hexagonal convection patterns and their evolutionary scenarios in electroconvection induced by a strong unipolar injection, Phys. Rev. Fluids **3**, 053702 (2018).
[23] A. Kourmatzis and J. Shrimpton, Turbulent three-dimensional dielectric electrohydrodynamic convection between two plates, J. Fluid Mech. **696**, 228 (2012).
[24] M. Zhang, Weakly nonlinear stability analysis of subcritical electrohydrodynamic flow subject to strong unipolar injection, J. Fluid Mech. **792**, 328 (2016).
[25] T.-F. Li, J. Wu, K. Luo, and H.-L. Yi, Lattice Boltzmann simulation of electro-hydro-dynamic (EHD) natural convection heat transfer in horizontal cylindrical annuli, Int. Commun. Heat Mass Transfer **98**, 106 (2018).
[26] C.-L. Lu, K. Luo, P.-C. Zhou, and H.-L. Yi, Lattice Boltzmann analysis for electro–thermo-convection with a melting boundary in horizontal concentric annuli, Phys. Fluids **33**, 043605 (2021).
[27] S. Oliveri and P. Atten, The linear stability of a spherical liquid layer subjected to a unipolar charge injection, Phys. Fluids **29**, 1378 (1986).
[28] P. Atten and R. Moreau, Stabilité électrohydrodynamique des liquides isolants soumis à une injection unipolaire, J. Mec. **11**, 471 (1972).
[29] J. Lacroix, P. Atten, and E. Hopfinger, Electro-convection in a dielectric liquid layer subjected to unipolar injection, J. Fluid Mech. **69**, 539 (1975).
[30] P. Atten and J. Lacroix, Non-linear hydrodynamic stability of liquids subjected to unipolar injection, J. Mec. **18**, 469 (1979).
[31] P. Atten, Electrohydrodynamic instability and motion induced by injected space charge in insulating liquids, IEEE Trans. Dielectr. Electr. Insul. **3**, 1 (1996).
[32] P. Atten and L. Elouadie, EHD convection in a dielectric liquid subjected to unipolar injection: Coaxial wire/cylinder geometry, J. Electrost. **34**, 279 (1995).
[33] D. V. Fernandes, H.-D. Lee, S. Alapati, and Y. K. Suh, Numerical simulation of the electro-convective onset and complex flows of dielectric liquid in an annulus, J. Mech. Sci. Technol. **26**, 3785 (2012).
[34] D. V. Fernandes, H.-D. Lee, S. Park, and Y. K. Suh, Electrohydrodynamic instability of dielectric liquid between concentric circular cylinders subjected to unipolar charge injection, J. Mech. Sci. Technol. **27**, 461 (2013).
[35] W. Hassen, M. Borjini, P. Traoré, and H. B. Aissia, Electroconvection between coaxial cylinders of arbitrary ratio subjected to strong unipolar injection, J. Electrost. **71**, 882 (2013).
[36] J. Huang, R. D. Selvakumar, Y. Guan, H. Li, P. Traoré, and J. Wu, Numerical investigation of injection-induced electro-convection in a dielectric liquid between two eccentric cylinders, Int. J. Heat Fluid Flow **83**, 108594 (2020).
[37] J. Huang, Q. Wang, Y. Guan, Z. Du, R. Deepak Selvakumar, and J. Wu, Numerical investigation of instability and transition to chaos in electro-convection of dielectric liquids between concentric cylinders, Phys. Fluids **33**, 044112 (2021).
[38] C. D. Dimitropoulos, R. Sureshkumar, and A. N. Beris, Direct numerical simulation of viscoelastic turbulent channel flow exhibiting drag reduction: Effect of the variation of rheological parameters, J. Non-Newton. Fluid Mech. **79**, 433 (1998).
[39] K. Weissenberg, A continuum theory of rheological phenomena, Nature (London) **159**, 310 (1947).

[40] A. N. Morozov and W. van Saarloos, An introductory essay on subcritical instabilities and the transition to turbulence in visco-elastic parallel shear flows, Phys. Rep. **447**, 112 (2007).
[41] C. P. Carroll and Y. L. Joo, Electrospinning of viscoelastic Boger fluids: Modeling and experiments, Phys. Fluids **18**, 053102 (2006).
[42] Z.-G. Su, T.-F. Li, K. Luo, and H.-L. Yi, Nonlinear behavior of electrohydrodynamic flow in viscoelastic fluids, Phys. Rev. Fluids **6**, 093701 (2021).
[43] G. Li, L. A. Archer, and D. L. Koch, Electroconvection in a Viscoelastic Electrolyte, Phys. Rev. Lett. **122**, 124501 (2019).
[44] D.-L. Chen, K. Luo, J. Wu, and H.-L. Yi, Electrohydrodynamic conduction pumping of a viscoelastic dielectric fluid with the Onsager–Wien effect, Phys. Fluids **33**, 113101 (2021).
[45] A. Pérez and A. Castellanos, Role of charge diffusion in finite-amplitude electroconvection, Phys. Rev. A **40**, 5844 (1989).
[46] N. Agrait and A. Castellanos, Linear convective patterns in cylindrical geometry for unipolar injection, Phys. Fluids A **2**, 37 (1990).
[47] R. Tobazeon, Electrohydrodynamic instabilities and electroconvection in the transient and AC regime of unipolar injection in insulating liquids: A review, J. Electrost. **15**, 359 (1984).
[48] J. Favero, A. Secchi, N. Cardozo, and H. Jasak, Viscoelastic flow analysis using the software OpenFOAM and differential constitutive equations, J. Non-Newton. Fluid Mech. **165**, 1625 (2010).
[49] F. Pimenta and M. Alves, Stabilization of an open-source finite-volume solver for viscoelastic fluid flows, J. Non-Newton. Fluid Mech. **239**, 85 (2017).
[50] J. P. Van Doormaal and G. D. Raithby, Enhancements of the SIMPLE method for predicting incompressible fluid flows, Numer. Heat Transfer **7**, 147 (1984).
[51] R. Fattal and R. Kupferman, Time-dependent simulation of viscoelastic flows at high Weissenberg number using the log-conformation representation, J. Non-Newton. Fluid Mech. **126**, 23 (2005).
[52] R. Comminal, J. H. Hattel, M. A. Alves, and J. Spangenberg, Vortex behavior of the Oldroyd-B fluid in the 4-1 planar contraction simulated with the streamfunction–log-conformation formulation, J. Non-Newton. Fluid Mech. **237**, 1 (2016).
[53] M. Alves, P. Oliveira, and F. Pinho, A convergent and universally bounded interpolation scheme for the treatment of advection, Int. J. Numer. Methods Fluids **41**, 47 (2003).
[54] J. Wu, P. Traoré, A. T. Pérez, and P. A. Vázquez, On two-dimensional finite amplitude electro-convection in a dielectric liquid induced by a strong unipolar injection, J. Electrost. **74**, 85 (2015).
[55] R. G. Larson, Instabilities in viscoelastic flows, Rheol. Acta **31**, 213 (1992).
[56] Y. Dubief and V. E. Terrapon, Heat transfer enhancement and reduction in low-Rayleigh number natural convection flow with polymer additives, Phys. Fluids **32**, 033103 (2020).
[57] R. J. Poole, M. A. Alves, and P. J. Oliveira, Purely Elastic Flow Asymmetries, Phys. Rev. Lett. **99**, 164503 (2007).